ARMY RESEARCH LABORATORY

Energetic Material Detection by Laser Photofragmentation-Fragment Detection (PF-FD) Spectroscopy

by Stephen D. Roberson and Rosario C. Sausa

ARL-TR-5244 **August 2010**

NOTICES

Disclaimers

The findings in this report are not to be construed as an official Department of the Army position unless so designated by other authorized documents.

Citation of manufacturer's or trade names does not constitute an official endorsement or approval of the use thereof.

Destroy this report when it is no longer needed. Do not return it to the originator.

Army Research Laboratory
Aberdeen Proving Ground, MD 21005-5069

ARL-TR-5244 **August 2010**

Energetic Material Detection by Laser Photofragmentation-Fragment Detection (PF-FD) Spectroscopy

Rosario C. Sausa
Weapons and Materials Research Directorate, ARL

Stephen D. Roberson
National Research Council
Postdoctoral Research Associateship Programs

REPORT DOCUMENTATION PAGE	Form Approved OMB No. 0704-0188

1. REPORT DATE *(DD-MM-YYYY)*	2. REPORT TYPE	3. DATES COVERED (From - To)
August 2010	Final	January 2009–Present

4. TITLE AND SUBTITLE
Energetic Material Detection by Laser Photofragmentation-Fragment Detection (PF-FD) Spectroscopy

5a. CONTRACT NUMBER

5b. GRANT NUMBER

5c. PROGRAM ELEMENT NUMBER

6. AUTHOR(S)
Stephen D. Roberson and Rosario C. Sausa

5d. PROJECT NUMBER

5e. TASK NUMBER

5f. WORK UNIT NUMBER

7. PERFORMING ORGANIZATION NAME(S) AND ADDRESS(ES)
U.S. Army Research Laboratory
ATTN: RDRL-WML-B
Aberdeen Proving Ground, MD 21005-5069

8. PERFORMING ORGANIZATION REPORT NUMBER
ARL-TR-5244

9. SPONSORING/MONITORING AGENCY NAME(S) AND ADDRESS(ES)

10. SPONSOR/MONITOR'S ACRONYM(S)

11. SPONSOR/MONITOR'S REPORT NUMBER(S)

12. DISTRIBUTION/AVAILABILITY STATEMENT
Approved for public release; distribution is unlimited.

13. SUPPLEMENTARY NOTES

14. ABSTRACT
We detect thin films of 2,4,6-trinitrotoluene (TNT) and hexahydro-1,3,5-hexanitro-1,3,5-triazine (RDX) by one- and two-laser photofragmentation (PF) with subsequent fragment detection in real time at ambient temperature and pressure. In the one-laser technique, a laser tuned to 226 nm excites the energetic material and both generates the characteristic nitric oxide (NO) photofragments and facilitates their detection by resonance-enhanced multiphoton ionization (REMPI) using their A-X (0,0) transitions near 226 nm. In contrast, in the two-laser technique, a 454-nm laser generates the analyte molecule in the gas phase by matrix assisted desorption, and a second laser tuned to 226 nm both photofragments it and ionizes the resulting NO. We report the effects of laser energy, analyte concentration, and matrix concentration on the ion signal and determine the rotational temperatures of the NO photofragments from Boltzmann, rotational distribution analysis of the REMPI spectra. We achieve limits of detection (LOD) (S/N=3) of hundreds of ng/cm^2 for both techniques under ambient conditions with a positive signal identification as low as 70 pg using a single, 226-nm laser pulse of about 50 μJ.

15. SUBJECT TERMS
energetic materials, laser photofragmentation-fragment detection

16. SECURITY CLASSIFICATION OF:			17. LIMITATION OF ABSTRACT	18. NUMBER OF PAGES	19a. NAME OF RESPONSIBLE PERSON
a. REPORT	b. ABSTRACT	c. THIS PAGE			Rosario C. Sausa
Unclassified	Unclassified	Unclassified	UU	28	19b. TELEPHONE NUMBER (*Include area code*) 410-306-0660

Standard Form 298 (Rev. 8/98)
Prescribed by ANSI Std. Z39.18

Contents

List of Figures

Acknowledgments

We thank Dr. Rose Pesce-Rodriguez for providing us with the 2,4,6-trinitrotoluene (TNT) and hexahydro-1,3,5-hexanitro-1,3,5-triazine (RDX) samples and Dr. Michael Grams for his invaluable assistance. Also, we thank Mr. Matthew Bratcher and Ms. Kristin Denault for the use of their profilometer, and Mr. Donovan Harris for the use of his imaging microscope. Support from the National Research Council Postdoctoral Research Associateship Program is greatly appreciated by Dr. Stephen Roberson.

INTENTIONALLY LEFT BLANK.

1. Introduction

Now more than ever, the detection of energetic materials is vital to the safety and security of the world. A device that is sensitive, accurate, robust, and detects hexahydro-1,3,5-hexanitro-1,3,5-triazine (RDX), 2,4,6-trinitrotoluene (TNT), as well as other energetic materials in real time under ambient conditions would be invaluable in both military and civilian applications. Lasers are widely used in and outside the laboratory for their ability to detect accurately low concentrations of energetic materials in real time under ambient conditions. Laser induced breakdown spectroscopy (LIBS) (*1*−*2*), Raman spectroscopy (*3*–*5*), and laser photofragmentation-fragment detection (PF-FD) (*6*–*19*) are three laser spectroscopic methods employed for energetic materials detection. LIBS uses high-powered, focused laser beams to completely break down a complex energetic material into its constituent elements. In contrast, Raman spectroscopy uses a laser to probe the molecule's vibrational and rotational states from the inelastic scatter of photons. When using LIBS as a detection technique, the breakdown of energetic material into atomic constituents can hinder positive energetic material identification. In contrast, PF-FD breaks down the complex explosive molecule into larger fragments or signature molecular groups that are subsequently detected, thus indicating the presence of the energetic material. When using Raman spectroscopy as a detection technique, the spectroscopic signal from a complex, energetic molecule like RDX or TNT is weak and difficult to interpret without additional computing hardware. In contrast, PF-FD produces small, signature molecules, whose spectra are relatively easy to interpret.

PF-FD detects energetic molecules by photofragmenting them into specific, characteristic molecular fragments and facilitating their detection by chemiluminecence (*8*), resonance-enhanced multiphoton ionization (REMPI) (*7*–*15*), or laser induced fluorescence (LIF) (*16*–*19*). This technique is extremely effective for nitro-containing, energetic molecules because they contain the characteristic nitro groups ($-NO_2$) that are easily fragmented from the energetic molecule. The structural formulas of RDX and TNT are shown in figure 1. Oftentimes, when the energetic molecule is excited in the ultraviolet (UV), nitric oxide (NO) molecules are readily generated directly from the energetic molecule or indirectly from the displaced nitrogen dioxide (NO_2) molecules. The ability to identify the signature NO photofragments allows the device to detect a number of energetic materials with similar molecular characteristics.

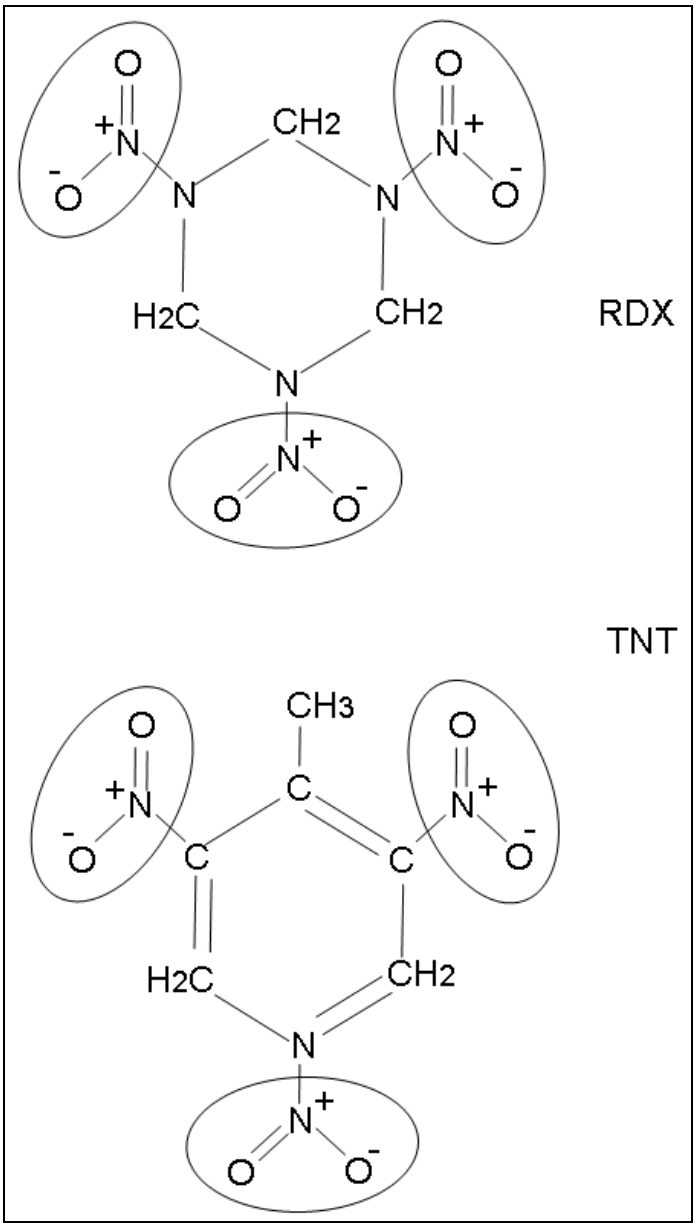

Figure 1. Structural diagram of RDX (top) and TNT (bottom). The outlying NO_2 groups are the signature functional groups for energetic material detection.

In a one-laser, PF-FD technique, the laser photolyzing the energetic molecule also excites the resulting characteristic NO photofragment, which is detected subsequently by LIF, REMPI, or both. Each fragment detection method has its advantages and shortcomings. Both LIF and REMPI offer high sensitivity, ease of setup, and the ability for concentration and temperature measurements in real time. LIF is an optical technique that allows for remote detection, whereas REMPI requires an ion probe and, thus, is more conducive for *in-situ* detection. However, research on the remote sensing of explosives by PF-FD with NO REMPI detection is ongoing (*20*). One significant challenge when trying to use LIF to detect energetic materials under

ambient conditions is collisional quenching. Molecular collisions quench electronically excited NO making it more difficult to detect at atmospheric pressure. REMPI mitigates this problem to a large extent because the ionization process is much faster than the collision quenching process. The ability to detect NO using LIF depends on the quantum efficiency of the optical detector, as well as the overall transmission efficiency of the monochromator or filter. The LIF and REMPI signals are both isotropic. However, a LIF detector captures only a portion of the emission, an amount related to the solid angle of the optical arrangement, whereas a REMPI probe captures nearly all of the resulting ions or electrons formed between metal plates. Thus, REMPI is, in general, a more sensitive technique than LIF for detecting equal amounts of NO generated from the energetic molecule at atmospheric pressure.

The vapor pressures of RDX and TNT, as well as may other energetic materials, are very low under ambient conditions. RDX's concentration is 6−30 parts per trillion by volume (ppt/v) and that of TNT is about 1 part per billion by volume (ppb/v) at 298 K and 1 atm (*21*−*22*). The low numbers of airborne energetic particles created naturally under ambient conditions challenge the sensitivity limit achievable by PF-FD and other techniques. Surface PF-FD increases substantially the number of airborne energetic molecules or characteristic fragments by laser heating, vaporization, or surface photolysis (*7*− *8*, *16*−*17*). Cabalo and Sausa reported the PF-FD detection of TNT, RDX, octohydro-1,3,5,7-octonitro-1,3,5,7-octazocine (HMX), and hexanitrohexazaisowurtzitane (CL20) residues under ambient conditions (*7*− *8*). A laser operating at either 248, 266 or 308 nm vaporized and/or photofragmented the target molecule and a second laser tuned to 226 nm ionized the characteristic NO fragment by REMPI by means of its A-X (0,0) transitions. They found that RDX's sensitivity is higher at 248 nm compared to 266 or 308 nm because its absorption coefficient is greater at 248 nm than the other two wavelengths (*7*). They determined the limits of detection (LOD) (S/N=3) to be in the range of 1 to 15 ng/cm^2 at 1 atm and 298 K, and found them to depend on the electrode orientation and mechanism for NO formation. The sensitivities of RDX and HMX are comparable, and they are higher than those of TNT and CL20 (*8*).

Wynn and coworkers detected a number of energetic molecules including TNT and RDX in the condensed phase under ambient conditions (*19*). One laser both vaporized and photolyzed the energetic material and also facilitated the detection of the resulting NO fragment by LIF. They excited NO by means of its A-X (0-1) and (0-2) transitions at 236 and 247 nm, respectively, and monitored its A-X (0,0) band at 226 nm for fluorescence detection. They probed NO's vibrational excited states to minimize any interference from ambient NO ($v''=0$) that may be present in the atmosphere. They determined that NO is formed predominantly in its $v''=1$ state compared to its $v''=2$ state with a rotational temperature, $T_r \sim 1000 \pm 500$. They detected 20 ng of TNT with each 236-nm laser pulse and reported that its signal is comparable to that of RDX above 5mJ/cm^2, but less than that of RDX at lower fluences.

Bernstein and his group studied the laser photolysis of a variety of energetic molecules with subsequent NO REMPI and time-of-flight mass spectrometric detection under vacuum

conditions. They employed both ns and fs lasers operating in the region of 226−258 nm for PF-FD (*11–15*). A 532-nm laser generated the target molecule in the gas phase by Matrix Assisted Laser Desorption (MALD) using R6G dye as the absorption medium, and a UV laser facilitated its detection by PF-FD. They determined that NO is the predominant product formed in a fast decomposition process, 180 fs, the time of their laser pulse. The nascent NO fragment is formed vibrationally hot (T_v ~1800K) and rotationally cold (T_r ~20K). Its signal from RDX:HMX:CL20 is in the ratio of 3:4:6, which corresponds to the number of NO_2 in each respective precursor molecule.

In this report, we report the detection of thin films of RDX and TNT in real time under ambient conditions using both two lasers and a single laser. In the two-laser setup, a 454-nm laser vaporizes mostly the energetic material by MALD and a 226-nm laser both photolizes the gas phase molecules and ionizes the resulting NO signature photofragments. In contrast, in the one-laser setup, a 226-nm laser both generates the NO photofragments and facilitates their detection by REMPI at or on the substrate's surface. We will report the effects of laser energy and analyte concentration on the signal strength, our NO rotational, temperature measurements and the limits of detection of TNT and RDX for both laser setups. In addition, we will show the effectiveness of MALD of TNT and RDX under ambient conditions at wavelengths where their absorption coefficients are very low.

2. Experimental Setup

Figure 2 is a schematic of the experimental apparatus for both the one- and two-laser setup. An optical parametric oscillator (OPO) (Continuum Sunlite[1] EX) pumped by a Nd:YAG laser (Continuum Powerlite[2] Precision II) generates the 454-nm laser output, and the frequency doubled output of a dye laser (Lumonics Hyperdye and Hypertrack) pumped by a Nd:YAG laser (Continuum Surelite[3] II) generates the tunable UV laser output near 226 nm. The laser output is 10 mJ/pulse at 454 nm and 20−50 μJ at 226 nm. Both lasers systems operate at a repetition rate of 10 pulses per second (pps) and each pulse is about 6 ns. The UV laser's linewidth is about 0.15 cm^{-1} near 226 nm. We use a Newport (935-10) attenuator to vary the energy for our study of laser energy on detection efficacy.

The REMPI probe is fabricated in-house. It contains two metals plates that are 1.3 cm by 2 cm in size, each with about a 3-mm hole in the center that allows the pump beam to pass through and strike the surface. The plates are 4 mm apart from each other, and the lower plate is about 1 mm from the substrate's surface. We estimate the electric field to be about 250 V/mm for a 1000-V

[1] Sunlite is a registered trademark of Continuum, Inc.

[2] Powerlite is a registered trademark of Continuum, Inc.

[3] Surelite is a registered trademark of Continuum, Inc.

bias between the plates. A current amplifier (Keithley 427, gain 10^6-10^7 V/A, time constant 0.01 ms) amplifies the signal, which we then feed to a 125-MHz oscilloscope (LeCroy 9400) for display. A personal computer records the signals from a boxcar averager (Stanford Research Systems, SR250). We use a digital delay generator (DDG) (Stanford Research Systems, DG535) to trigger the UV laser to fire after the visible laser, as well as to control the time delay between the pump and probe lasers. The time delay between the two lasers is typically 100 μs.

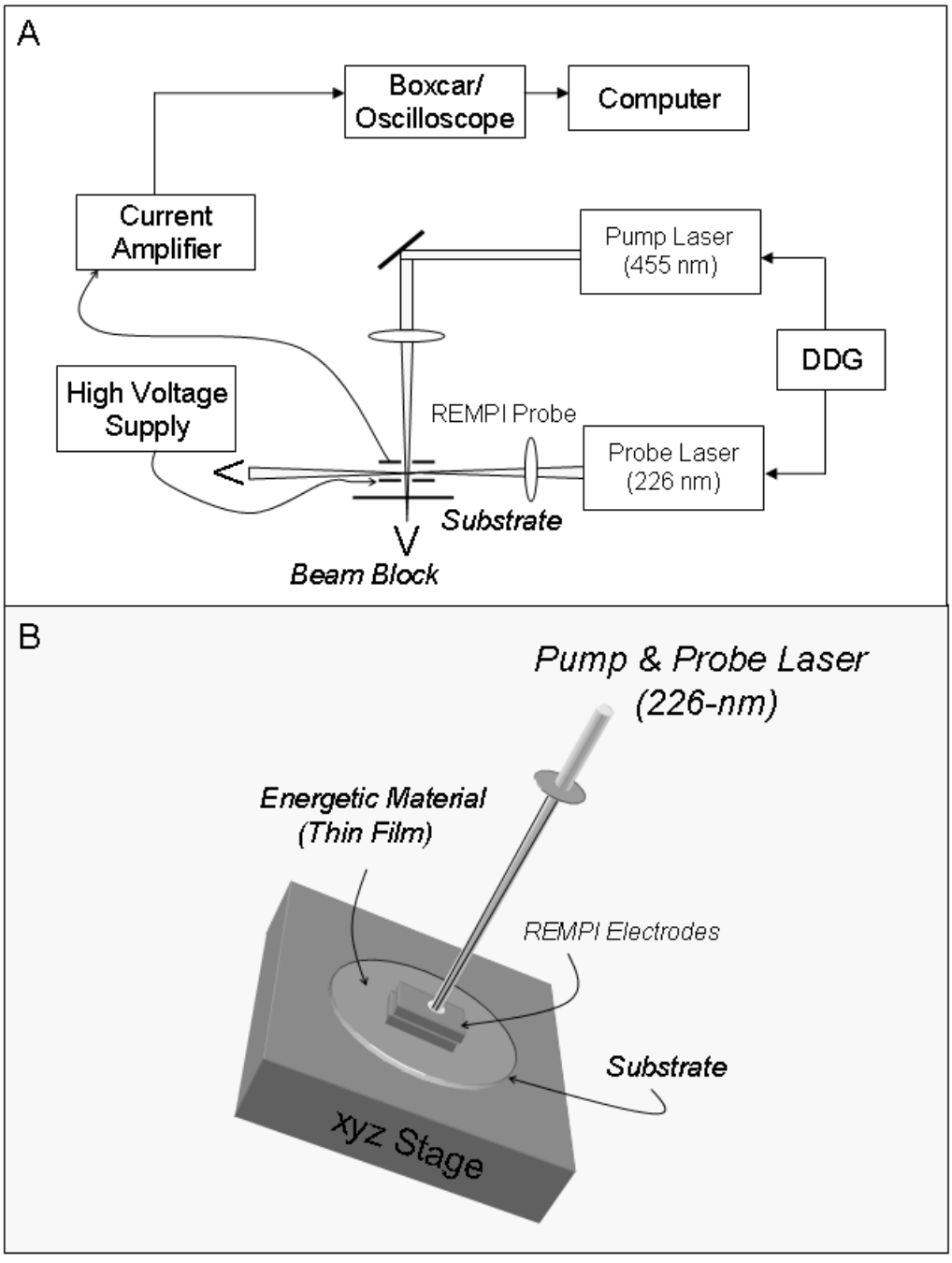

Figure 2. Diagrams of experimental setup for the two-laser (top) and one-laser (bottom) setup.

In the two-laser setup, we focus the visible beam with a 200-mm lens, 30 mm below the quartz substrate containing a thin-film matrix of RDX or TNT and laser dye in order to avoid any plasma formation on the sample. We then direct the UV laser beam, which we focus with a 100-mm focal length lens, between the REMPI plates. The UV beam is normal to the visible beam about 3 mm from the quartz surface. In contrast, in the one-laser setup, we utilize only the UV laser beam. We focus it approximately 1 mm above the quartz's surface, near the bottom of the REMPI plate. We do not observe any plasma formation on the substrate's surface because the UV laser flux is sufficiently low under our experimental conditions.

We prepare the thin films by coating circular, quartz plates with known concentrations of energetic material/methanol solution and then evaporating the solvent with a hotplate. A personal computer that is interfaced with an XYZ stage (Anaheim Automation LS100 series) allows for precise programmable movement of the substrate. Typical scan speeds range from 0.1 to 0.2 mm/s. We record excitation scans by scanning the UV laser over the region 226.5 to 227.3 nm at a speed of 0.025 nm/s with 10-shot averaging. We average three to five scans to account for any variation for film thickness during each scan. We determine the technique's sensitivity by recording the REMPI response of NO from TNT or RDX, neat or in a matrix with equimolar coumarin dye C540A (Exciton), at various surface concentrations. C540A's strong, broad absorption band in the visible, which peaks at 423 nm, makes it suitable for our 454-nm MALD process. Research on substituting the laser dye with energetic binders in the matrix is ongoing. For the limit of detection and the laser energy measurements, the UV laser beam is tuned near 226.8 nm and collect 8000 data points for each measurement to obtain average values and standard deviations of the REMPI signal.

Our colleagues at the U.S. Army Research Laboratory (ARL) provided us with the RDX and TNT samples. RDX is about 98% pure and TNT is military grade. Our methanol is from Alpha Aesar (High Performance Liquid Chromatography [HPLC] grade) and NO gas from Airgas (0.097% in Argon [Ar]). We use a profilometer to measure the thickness of the films and an imaging microscope to observe and photograph the various laser-induced features on the substrate's surface.

3. Results and Discussion

3.1 Two-Laser Experiments (454 nm + 226 nm)

Figure 3 shows REMPI spectra of NO from TNT or RDX generated by exciting the thin-film matrix at 454 nm, while scanning the 226-nm laser at 1 atm and 298K. The figure also shows a reference REMPI spectrum of room temperature NO gas in a flow cell. A comparison of the spectra reveals that the spectral features of NO from TNT and RDX are very similar to those of ambient NO, indicating successful formation of NO with its subsequent selective ionization. The

two broad TNT and RDX peaks near 226.80 and 226.93 nm are due to NO A-X (0,0) rotational lines forming the P_2 and Q_2 bandheads and the P_{12} subband, respectively. The bands show rotational structure with sufficient spectral resolution to resolve some of the rotational lines even at 1 atm. We do not observe any REMPI signal from NO when the visible laser is on and the UV laser radiation is tuned off an NO transition. Also, we do not observe any NO REMPI signal from TNT or RDX without dye under our experimental conditions. Neat TNT and RDX films are very weak absorbers at 454 nm, and the laser fluence is sufficiently low as not to cause any laser desorption under our experimental conditions. Our observations reveal that only the UV laser beam causes ionization of NO. The visible laser beam does not generate NO from direct excitation of the energetic material or through any energy transfer processes from the dye to the energetic material in the MALD process. Our results corroborate previous results that show that the MALD of energetic materials can be performed successfully to generate volatile molecules with minimal ionization or fragmentation (*11–15*, *23*).

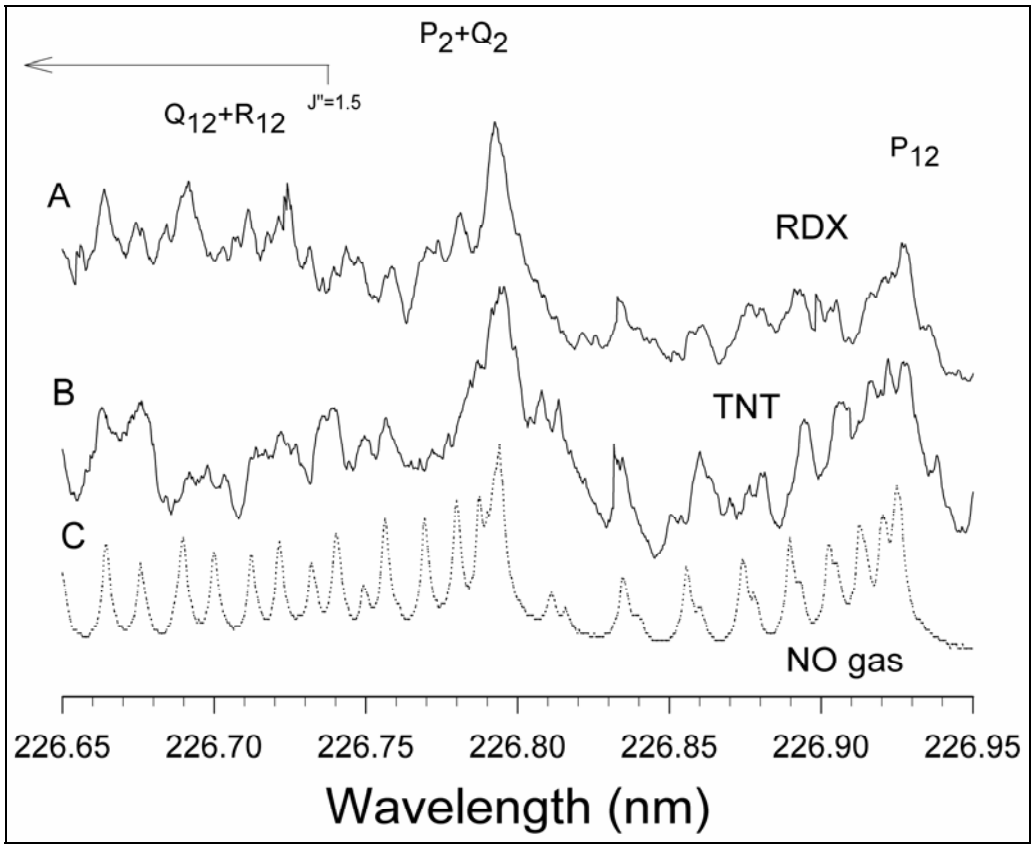

Figure 3. Two-laser REMPI spectra of RDX (A), TNT (B), and reference NO (C).

Figure 4 shows the observed and calculated REMPI spectra of room temperature NO (A) and NO from TNT-dye film (B) in the region of 226.6 to 226.95 nm. We calculate the NO spectrum with a multi-parameter, computer program based on a Boltzmann, rotational line analysis of NO (*7–8*). We input the rotational energies and line strengths of NO into the program and vary the

temperature, concentration, baseline, laser linewidth, and laser line shape. The best fit to the observed TNT data yields a rotational temperature of 450 ± 50 K using a Gaussian function for the line shape. We obtain a comparable temperature for NO from RDX. A similar analysis of room temperature NO yields a temperature of 308 ± 15K. Our results suggest that NO is formed in the gas phase by the 226-nm photolysis of either a parent TNT or RDX molecule or some daughter species. If it is formed on or near the substrate's surface by laser-induced photochemical reaction at 454 nm or by surface-induced reactions, then it would be rotationally thermalized when we interrogate it with our probe laser, 100 μs after we fire our visible laser, about 3 mm above the substrate's surface at 1 atm.

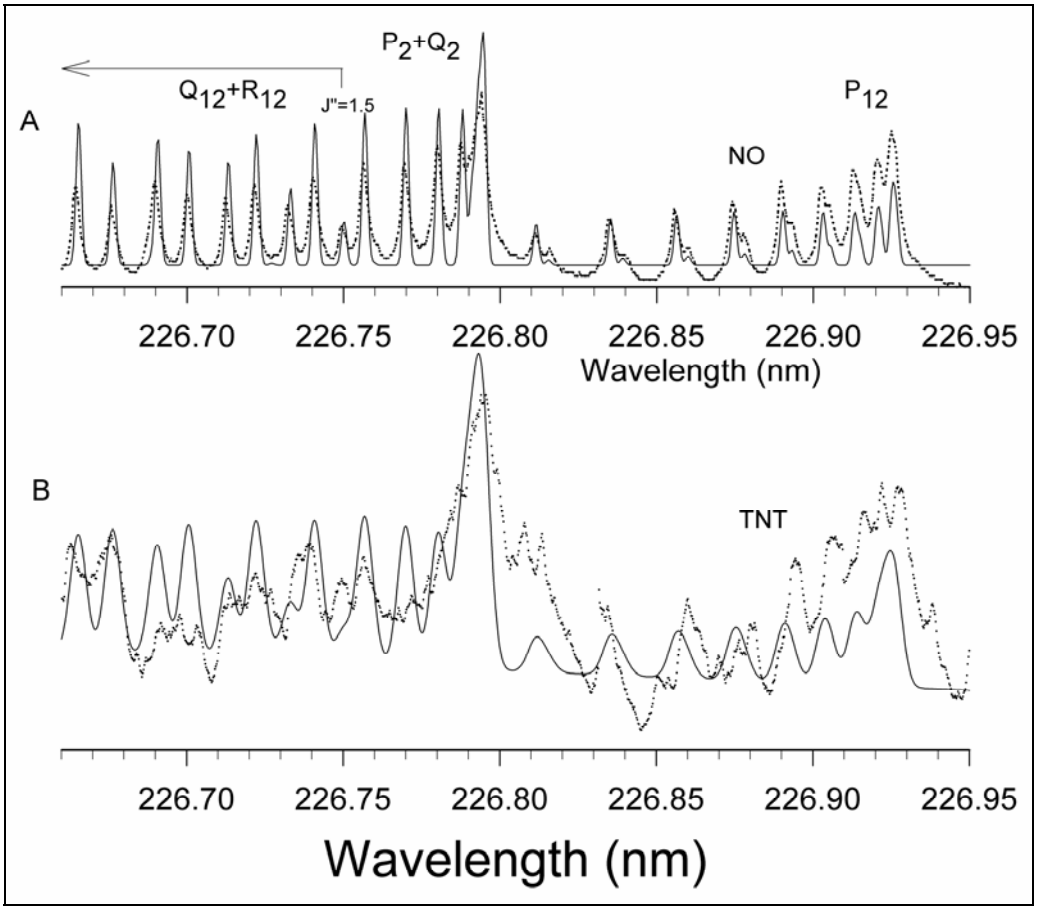

Figure 4. Observed and calculated REMPI spectra of NO (A) and NO from a TNT-dye matrix (B).

Wynn and coworkers report a NO rotational temperature of 1000K ± 500K in their one-laser, 237-nm PF-LIF of both TNT films, and bulk TNT and composition 4 (C4), an explosive material containing about 90% RDX (*19*). Their experimental uncertainty is in part due to their laser linewidth, 0.03-0.04 nm (5−7 cm^{-1}), which is about 30−50 times greater than our linewidth, 0.15 cm^{-1}. Thus, they are probing simultaneously many NO rotational lines with both low and high J-values. They claim that the NO temperature depends somewhat on morphology and laser

fluence (1−60 mJ/cm^2), with larger fluencies yielding hotter NO temperatures. Our fluence is about 23 mJ/cm^2 for comparison purposes. We derive this value using a laser energy of 50 μJ and a beam area of 2.2×10^{-5} m^2, which we obtain from the laser beam's Airy-disk diameter, $d = 2.44\lambda(f/D)$, where λ is the laser wavelength, f is the lens' focal length, and D the laser beam diameter. The NO temperatures may differ in the two experiments because each group probes the NO photofragment at different stages of its temperature history, from its initial formation with a nascent, rotational distribution to its eventual thermalization at room temperature. However, the observed temperatures differ probably because the photochemistry that governs the NO photofragnent is different in the two experiments. It is unlikely that the NO generation from TNT and RDX differs much at 237 nm compared to 226 nm. Thus, the main difference in the measurements is that we probe NO that is generated about 3mm away from the surface, presumably from a gas-phase, energetic parent molecule or its daughter species, whereas they probe NO that is generated near or at the surface, where surface-molecule reactions, laser-surface effects, or both, play a role in its formation. We will explore this point in the subsequent section of this report where we present our results on the one-laser, 226-nm excitation of neat, energetic, thin films on surfaces.

Bernstein and his group report a NO rotational temperature of 20K in their one-laser, PF-REMPI experiments of gas-phase RDX at 226 nm using laser fluencies in the range of 0.2−0.6 mJ/pulse (*14*). Their experimental conditions are very much different than ours and, as a result, different RDX photolysis mechanisms are in play. Their collisonless environment allows them to photolyze a single RDX molecule that is prepared rotationally cold because of its supersonic expansion into their vacuum chamber. These conditions will certainly influence the rotational distribution of the resulting NO photofragment, which they claim is a direct product of RDX decomposition from an isolated, electronic state molecule. In contrast, we perform our experiments in a collisional environment at room temperature, where collisions from other RDX molecules, intermediate molecules, as well as ambient nitrogen (N_2) and oxygen (O_2), play a role in the photodissociation dynamics. Also, the NO photofragment may result from a RDX daughter species, in addition to the parent RDX molecule, under our experimental conditions.

Figure 5 is a graph of NO signal strength vs. pump laser pulse energy for both RDX and TNT. The graph reveals that both signals decrease with decreasing pulse energy, as expected. It is interesting to note, however, that the NO REMPI signal from RDX is greater than that from TNT and that the ratio of the RDX to TNT signal increases as the laser energy decreases. A plot of signal strength vs. dye concentration for a given RDX or TNT concentration, not shown, shows that the signal decreases linearly with decreasing dye concentration. The effects of laser energy and dye concentration on REMPI signal are similar and suggest that lowering the dye concentrations is tantamount to decreasing the laser energy, both resulting in the dye absorbing less energy.

Figure 6 are images from the 454-nm laser removal of RDX and TNT from the substrate. The concentration of both RDX and TNT is about 3 μg/cm^2 and that of the dye is about 4.6 and 1.2

$\mu g/cm^2$ for the images on the left and right, respectively. The edges' location is somewhat arbitrary because it is not well defined. Nevertheless, we note that the width of the grooves created by the 454-nm laser decreases as the dye concentration decreases. The grooves created by the laser for both RDX and TNT further show the importance of efficient energy absorption of the thin-film matrix. The images show that the edges of TNT's grooves, and to some extent those of RDX, appear rough and not as uniform as the neat, non-irradiated film. These observations suggest that the energetic material or possibly the dye could be decomposing, resolidifying, or both, particularly at the laser beam's outskirt. Therefore, it is plausible that the laser beam's center, which contains the bulk of the energy, results in energetic material vaporization, whereas its outskirt, which contains less energy, causes melting, resolidification, or partial decomposition of the energetic material or dye. Scanning electron microscopy and chemical analyses of the samples, particularly the feature's edges, are ongoing.

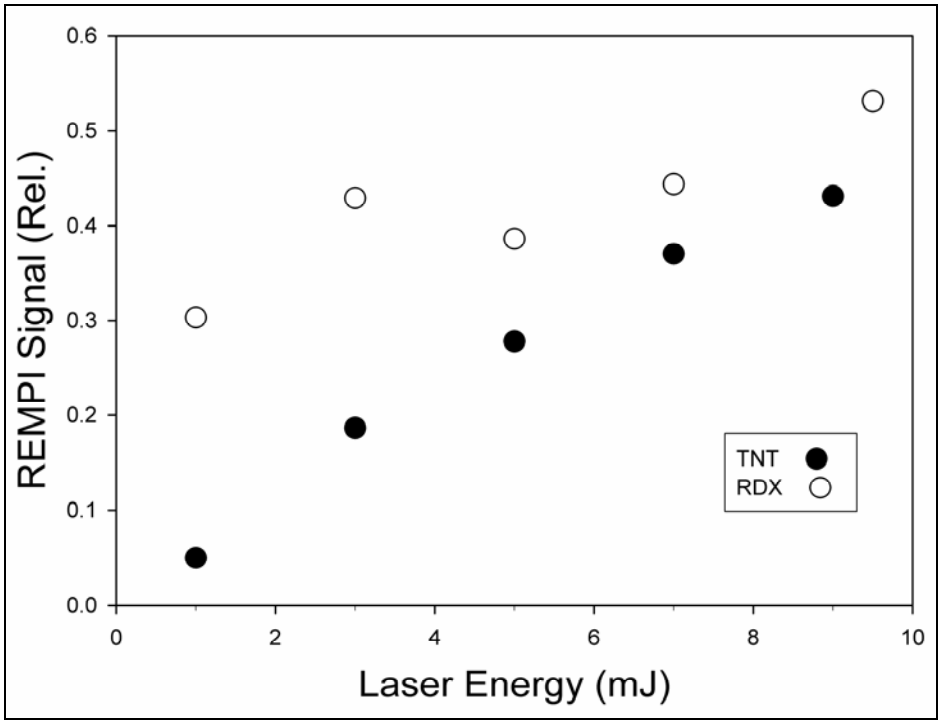

Figure 5. Signal strength vs. laser energy for fixed, surface concentrations of RDX and TNT under ambient conditions.

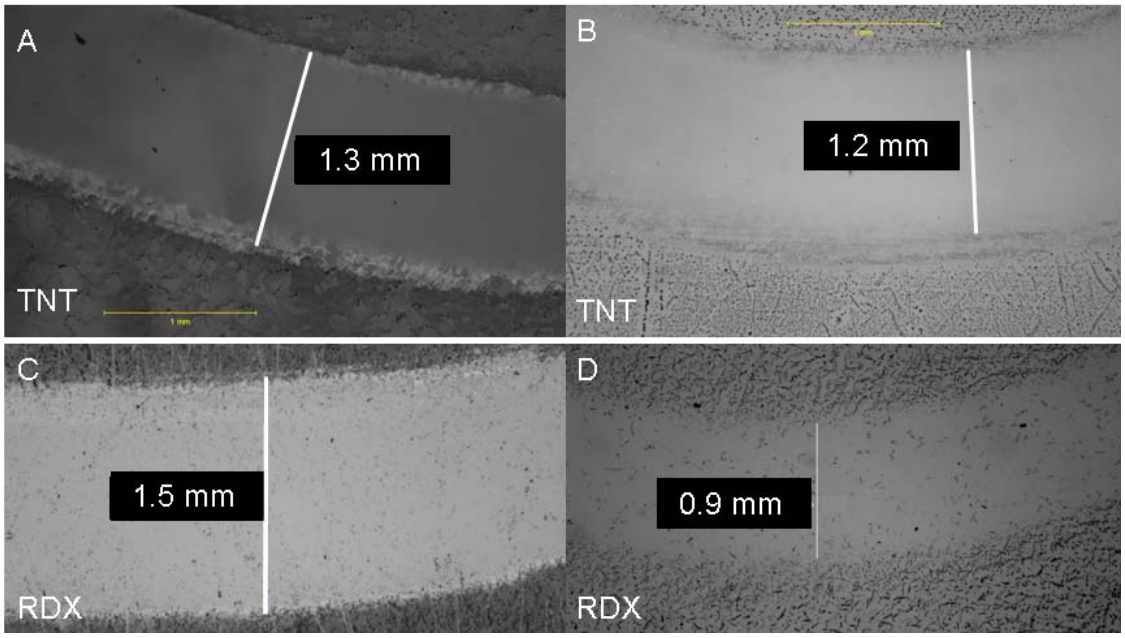

Figure 6. Photos of grooves created by the 454-nm laser MALD of RDX- and TNT-containing thin films with a TNT and RDX surface concentration of about 3 μg/cm^2 and dye concentration of about 4.6 μg/cm^2 (left) and 1.2 μg/cm^2 (right).

Figure 7 shows plots of NO signal response vs. RDX and TNT surface concentration. We determine the technique's analytical sensitivity by calculating the LODs, defined as $C_L = 3\sigma/R$, where C_L is the concentration, R is the signal response, and σ is the standard deviation of the background signal. The best fits of the signal response vs. concentration data, along with the noise measurements, yield RDX and TNT LODs of 400 and 543 ng/cm^2, respectively. The sensitivity values arise from a convolution of laser-induced photochemical, photothermal, and photophysical mechanisms leading ultimately to the ionization of NO. These complex mechanisms must include the condensed phase, MALD process where the dye absorbs the laser radiation and transfers it to the energetic material, causing it to vaporize, and must account for any dye and/or energetic material melting, sublimation, or decomposition. In the gas phase, the absorption coefficients of RDX and TNT are important at 226 nm, as is their photochemistry and the role of collisions from other parent molecules, photolytic intermediates, ambient O_2 and N_2, or combination thereof, on their photodissociation and NO generation. Our results show that RDX exhibits a higher sensitivity than TNT. These results are consistent with those obtained previously by our group and other research groups under a variety of experimental conditions (*6−7, 9, 19*). However, our sensitivity is much lower than that achieved in our laboratory using a 248-nm laser to excite neat RDX or TNT, and a 226-nm laser for probing the resulting NO fragments. If we account for the differences in the probe's electrode field, rotational line probed, and laser energy at 226 nm, the major difference in the sensitivities stems from using a different laser-excitation wavelength and exciting the energetic materials in a matrix. The different experimental conditions suggest two distinct mechanisms for NO

generation. The 248-nm laser excites the neat energetic material and produces both photofragments and molecular ions (*7*, *24*). The NO photofragments have a rotational temperature of 325K, which indicates that they are rotationally equilibrated by the time they are probed by the 226-nm laser (*7*). This suggests that the NO photofragments are generated from the 248-nm laser radiation on or near the substrate's surface and that the 226-nm laser radiation acts as a probe, instead of photolizing any resulting gas-phase parent or daughter species that the 248-nm laser generates. In contrast, the 454-nm laser excites the dye, which in turn transfers its absorbed energy to the energetic material and causes it to vaporize mostly under our present measurements. Subsequently, the 226-nm laser both photolyzes the energetic molecule and excites the resulting NO fragments. The NO photofragments have a rotational temperature of 450K suggesting that they are thermalized partially under our experimental conditions. Neither the energetic material nor dye is ionized at 454 nm because we do not observe any ions with our electrodes, but they may decompose in part during the MALD process. However, if they do decompose in the MALD process, NO is not the main decomposition product. The NO fragments that we observe are generated mostly from the gas-phase photolysis of the parent molecule or daughter species that is a precursor to NO, as our spectral results indicate. Although we do not understand fully the mechanisms' intricacies for NO formation, the two-laser technique with NO REMPI detection is a viable method for detecting TNT and RDX residues *in situ* and in real time under ambient conditions.

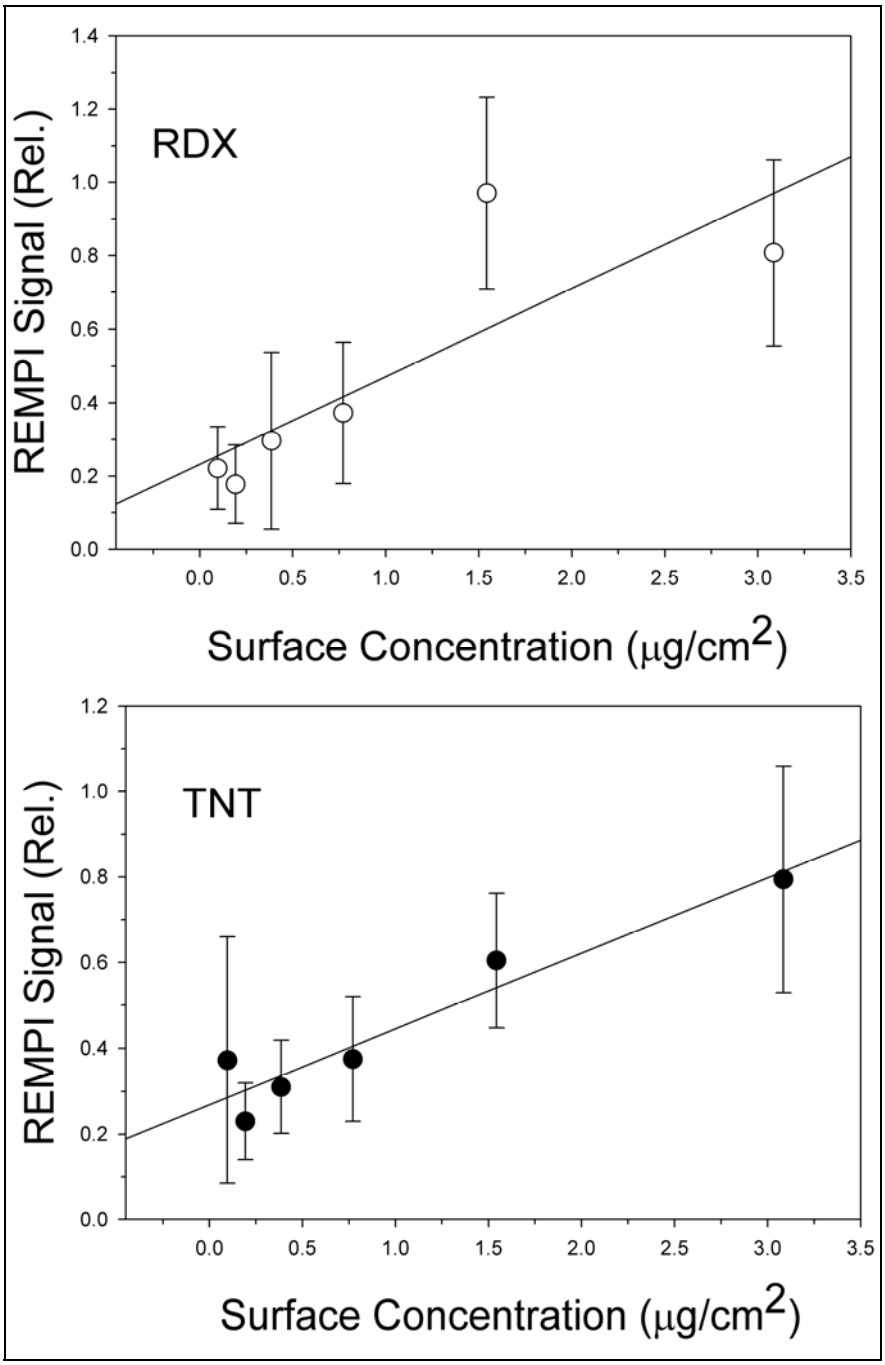

Figure 7. Two-laser, REMPI response plots of NO from RDX (top) and TNT (bottom) at 298K and 1 atm.

3.2 Single Laser Experiments (226 nm)

A one-laser setup is less complex than a two-laser setup for energetic material detection because it requires only one laser to both generate and ionize the resulting NO photofragments. In addition, aligning one laser beam spatially for signal optimization is simpler than aligning two laser beams both spatially and temporally for signal optimization. Figure 8 shows REMPI spectra of NO from neat, RDX (A) and TNT (B) films in the region of 226.65 to 226.95 nm using about 50 μJ of laser energy. The spectra are similar to those obtained with our two-laser setup and their spectral features result mainly from NO A-X (0,0) transitions of the P_2, Q_2, and P_{12} bands. Our results indicate successful generation of NO from the energetic material with subsequent selective ionization of NO. We do not observe any signal from NO when we detune the laser from the NO resonant transitions. Our results corroborate those reported by both our group and others (*10*, *11–15*, *19*, *25*). Figure 8C shows both our observed and calculated spectra for TNT. A Boltzmann population distribution analysis of the data yields a rotational temperature of 350 +/- 50 K. We obtain a similar temperature for RDX. Our results suggest that the NO fragments are generated near or at the substrate's surface and that collisonal energy transfer from other species equilibrates them to a near, room-temperature, rotational distribution about 1 mm above the surface. Wynn and coworkers report a NO temperature of 1000 K ± 500K from the one-laser, PF-FD of condensed-phase TNT and RDX, which suggests that they probe NO photofragments that are more nascent in the photodissociation process than ours.

We determine the technique's analytical sensitivity from our signal strength vs. concentration and noise measurements. Our analysis yields similar LODs (S/N=3) for RDX and TNT, in the range of 600−700 ng/cm^2 The laser fluence is about 10 mJ/cm^2 for a 226-nm beam with energy of about 50 μJ and a diameter of 2.6 x 10^{-5} m at 1 mm from the surface. We obtain the beam diameter from the beam's, Airy radius and estimating its variation along the z-axis by equation $R(z) = R_o [(1+ (Z(z)/Z_r)^2]^{1/2}$, where R_o is its radius at the z-axis origin, Zr, defined as $\pi R_o^2/\lambda$, where λ is the laser wavelength. Our RDX and TNT REMPI results are consistent with those from previous one-laser, PF-LIF studies (*19*). Wynn and coworkers find that the NO LIF signal from RDX and TNT depends on the laser fluence: RDX's sensitivity is greater than that of TNT for fluencies less than 5 mJ/cm^2, but it becomes fairly similar to that of TNT above 5mJ/cm^2, where some saturation occurs in TNT's NO LIF.

We are able to detect the energetic materials with a single, 226-nm laser shot. Five laser shots completely remove films that are 10 to 15 μ thick and contain 0.25 mg of RDX or TNT over an area of about 20 cm^2. The energetic material's removal volume ranges from 8×10^{-9} to 2.4×10^{-8} cm^3 for impact craters of 70 to 100 μ and a removal rate of 2 to 3 μ/pulse. This means that our one-laser REMPI system is able to detect NO fragments from 70 to 300 pg of energetic material using a single laser pulse with an energy of about 50 μJ. These values are comparable to the 200-pg value obtained for RDX by Raman microscopy (*5*), and RDX and TNT by laser desorption-ion mobility spectrometry (*23*), but lower than the 20-ng value obtained for TNT by PF-LIF (*19*).

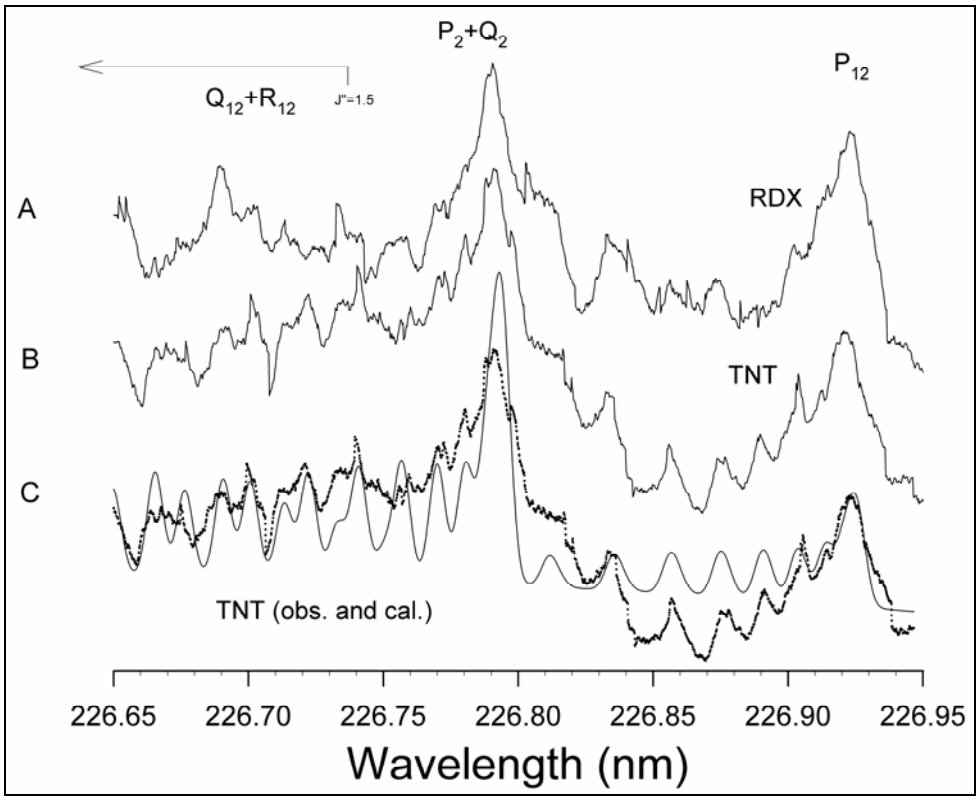

Figure 8. One-laser, REMPI spectra of NO from RDX (A) and TNT (B), and observed (….) and calculated (-) spectra of NO from TNT (C) in the region of 226.65 to 226.95 nm.

4. Conclusions

We have demonstrated the detection of TNT and RDX residues by one- and two-laser PF-FD employing REMPI of the signature, NO photofragment *in situ* and in real time under ambient conditions. The technique's analytical sensitivity depends on the photochemical and photothermal processes producing NO. Our NO rotational temperature measurements reveal that in the two-laser configuration, the 454-nm radiation vaporizes mostly the energetic material by MALD and the 226-nm laser radiation both generates and ionizes the resulting NO photofragments. In contrast, in the one-laser configuration, the 226-nm radiation excites the neat, energetic material and both facilitates its decomposition and the detection of the resulting NO photofragments on or near the substrate's surface. The limits of detection are 400 and 543 ng/cm^2 for RDX and TNT, respectively, for the two-laser configuration, and in the range of 600 to 700 ng/cm^2 range for both RDX and TNT for the one-laser configuration. We can detect as low as 70 pg of energetic material with a single pulse of low power, 226-nm radiation, and we anticipate that the technique's effectiveness can be increased with improvements in laser hardware. The technique is not restricted to TNT and RDX, and its extension to other energetic materials is ongoing.

5. References

1. Dikmelik, Y.; McEnnis, C.; Spicer, J. B. *Opt. Express* **2008**, *16*, 5332, and reference therein.
2. Munson, C. A.; Gottfried, J. L.; De Lucia, J. Frank C.; McNesby, K. L.; Miziolek, A. W. *Counterterrorist Detection Techniques of Explosives*, Yinon, J., Ed.; Elsevier B. V.: The Netherlands, 2007; p. 279, and references therein.
3. Comanescu, G.; Manka, C. K.; Grun, J.; Nikitin, S.; Zabetakis, D. *Appl. Spectrosc*. **2008**, *62*, 833, and references therein.
4. Carter, J. C.; Angel, S. M.; Lawrence-Snyder, M.; Scaffidi, J.; Whipple, R. E.; Reynolds, J. G. *Appl. Spectrosc*. **2005**, *59*, 769.
5. Cheng, C.; Kirkbride, T.; Batchelder, D.; Lacey, R.; Sheldon, T. *J. Forensic Sci*. **1995**, *40*, 31.
6. Monterola, M.; Smith, B.; Omenetto, N.; Winefordner, J. *Anal Bioanal Chem* **2008**, *391*, 2617.
7. Cabalo, J.; Sausa, R. *Appl. Opt*. **2005**, *44*, 1084.
8. J. Cabalo and R. Sausa, *Applied Spectroscopy* **2003**, *57* (9), 1196.
9. Lemire, G. W.; Simeonsson, J. B.; Sausa, R. C. *Anal. Chem*. **1993**, *65*, 529.
10. Simeonsson, J. B.; Sausa, R. C. *TrAC Trends in Analytical Chemistry* **1998**, *17*, 542.
11. Guo, Y.; Bhattacharya, A.; Bernstein, E. *J. Phys. Chem*. A **2009**, *113*, 85.
12. Im, H.; Bernstein, E. R. *J. Chem. Phys*. **2000**, *113*, 7911.
13. Guo, Y. Q.; Greenfield, M.; Bhattacharya, A.; Bernstein, E. R. *J. Chem. Phys*. **2007**, *127*, 154301.
14. Guo, Y.; Greenfield, M.; Bernstein, E. *Journal of Chemical Physics* **2005**, *122*, 244310.
15. Greenfield, M.; Guo, Y.; Bernstein, E. *Chem Phys. Letters* **2006**, *430*, 277.
16. Bourdreax, G.M.; Miller, T.S.; Kunefke, A. J.; Singh, J. P.; Yueh, F.; Monts, D. *Applied Optics* **1999**, *38*, 1411.
17. Heflinger, D.; Arusi-Parpar, T.; Ron, Y.; Lavi, R. *Opt. Commun*. **2002**, *204*, 327.
18. Arusi-Parpar, Heflinger, D.; Lavi, R. *Applied Optics*. **2001**, *40*, 6677.

19. Wynn, C. M.; Palmacci, S.; Kunz, R. R.; Clow, K.; Rothschild, M. *Appl. Opt*. **2008**, *47*, 5767.

20. Angel, S. M. Department of Chemistry and Biochemistry, University of South Carolina, Columbia, SC 29208. Private communication.

21. Dionne, B. C.; Rounbehler, D. P.; Achter, E. K.; Hobbs, J. R.; Fine, D. H. *Journal of Energetic Materials* **1986**, *4*, 447, and references therein.

22. Eiceman, A.; Preston, D.; Tiano, G.; Rodriguez, J.; Parmeter, J.E. *Talanta* **1997**, *45* (57).

23. Duo, S.; Kolaitis, L.; Lubman, D. *Applied Spectroscopy* **1987**, *41* (8), 1771.

24. Dikinson, J.; Jensen, L.; Doering, D.; Lee, R. *J. Applied Physics* **1990**, 67, 3641.

25. Tang, T.; Chaudhri, M.; Rees, C.; Mullock, S. *J. Material Science* **1987**, *22*, 1037.

List of Symbols, Abbreviations, and Acronyms

Ar	Argon
ARL	U.S. Army Research Laboratory
C4	composition 4
CL20	hexanitrohexazaisowurtzitane
DDG	digital delay generator
HMX	octohydro-1,3,5,7-octonitro-1,3,5,7-octazocine
HPLC	High Performance Liquid Chromatography
LIBS	laser induced breakdown spectroscopy
LIF	laser induced flourescence
LOD	limits of detection
MALD	Matrix-Assisted Laser Desorption
N_2	nitrogen
NO	nitric oxide
$-NO_2$	nitro group
NO_2	nitrogen dioxide
O_2	oxygen
OPO	optical parametric oscillator
PF	photofragmentation
PF-FD	photofragmentation-fragment detection
ppb/v	parts per billion per volume
ppt/v	parts per trillion per volume
pps	pulses per second
RDX	hexahydro-1,3,5-hexanitro-1,3,5-triazine
REMPI	resonance-enhanced multiphoton ionization
TNT	2,4,6-trinitrotoluene
UV	ultraviolet

NO. OF COPIES	ORGANIZATION
1 (PDF only)	DEFENSE TECHNICAL INFORMATION CTR DTIC OCA 8725 JOHN J KINGMAN RD STE 0944 FORT BELVOIR VA 22060-6218
1 HC	DIRECTOR US ARMY RESEARCH LAB IMNE ALC HRR 2800 POWDER MILL RD ADELPHI MD 20783-1197
1 HC	DIRECTOR US ARMY RESEARCH LAB RDRL CIM L 2800 POWDER MILL RD ADELPHI MD 20783-1197
1 HC	DIRECTOR US ARMY RESEARCH LAB RDRL CIM P 2800 POWDER MILL RD ADELPHI MD 20783-1197
1 HC	DIRECTOR US ARMY RESEARCH LAB RDRL D 2800 POWDER MILL RD ADELPHI MD 20783-1197
	ABERDEEN PROVING GROUND
1 HC	DIR USARL RDRL CIM G (BLDG 4600)

NO. OF
COPIES ORGANIZATION

1 HC DIR USARL
RDRL ROP TECH LIB
PO BOX 12211
RESEARCH TRIANGLE PARK NC
27709-2211

1 HC US ARMY
PEO AMMOO PMCAS
SFAE AMO CAS
J IRIZARRY
BLDG 171A
PICATINNY ARSENAL NJ 07806-5000

1 CD COMMANDER
RADFORD ARMY AMMO PLANT
SMCAR QA HI LIB
RADFORD VA 24441-0298

1 HC DIR BENET WEAPONS LAB
TECH LIB
WATERVLIET NY 12189-4000

1 HC CDR NAVAL RSRCH LAB
TECH LIB
WASHINGTON DC 20375-1972

ABERDEEN PROVING GROUND

7 HCs DIR USARL
RDRL WML
M ZOLTOSKI
RDRL WML B
B E HOMAN
R C SAUSA (3 CPS)
RDRL WML C
K L MCNESBY
RDRL WML D
R A BEYER

2 HCs DIR USARL
RDRL SEE O
N FELL
S ROBERSON
2800 POWDER MILL RD
ADELPHI MD 20783

2 HCs MASSACHUSETTS INST OF TECHLGY
M ROTHSCHILD
C W WYNN
LINCOLN LABORATORY
LEXINGTON MA 02420

NO. OF
COPIES ORGANIZATION

3 HCs PA STATE UNIVERSITY
K KUO
T LITZINGER
S THYNELL
DEPT OF CHEM ENGRG
UNIVERSITY PARK PA 16802

3 HCs UNIVERSITY OF FLORIDA
N OMENETTO
SMITH
WINEFORDNER
DEPT OF CHEMISTRY
GAINESVILLE FL 32611

1 HC UNIV OF SOUTH CAROLINA
S M ANGEL
DEPT OF CHEMISTRY AND
BIOCHEMISTRY
COLUMBIA SC 29208

3 HCs US ARMY EDGEWOOD CHEMICAL
BIOLOGICAL CTR
J CABALO
S CHRISTESEN
A W FOUNTAIN III
RSRCH AND TECHLGY DIRCTRT
EDGEWOOD MD 21010

1 HC US ARMY RSRCH OFC
RDRL ROP C
J PARKER
PO BOX 12211
RESEARCH TRIANGLE PARK NC
27709-2211